The Gaspé Current and Cyclonic Motion Over the Northwestern Gulf of St. Lawrence

Jinyu Sheng[1]

Abstract

A three dimensional primitive equation ocean model was used to study the dynamics of the Gaspé Current and cyclonic circulation over the northwestern Gulf of St. Lawrence. The model was first applied to the idealized basin with a flat bottom and a piecewise-straight coastline driven by buoyancy forcing associated with St. Lawrence River discharge. The model reproduces many known features in the early development of the estuary plume and the associated coastal current system. The coastal current, which flows seaward along the right-bounded coast on the northern Hemisphere, is stable initially but becomes unstable quickly with the occurrence of multiple backward-breaking waves as a result of momentum advection. The model was then applied to the realistic basin driven by the same buoyancy forcing. The early development of the plume-current system is qualitatively similar to that in the idealized basin. The combined effects of irregular bathymetry and momentum advection, however, make the intrusion advance considerable slower in the realistic basin than that in the idealized basin. The coastal current in the realistic basin separates from and reattaches to the coast sporadically as it propagates downstream.

Introduction

The Gaspé Current is a buoyancy-driven coastal jet originating in the St. Lawrence Estuary and flowing seaward along the coast of the Gaspé Peninsula

[1]Department of Oceanography, Dalhousie University, Halifax, Nova Scotia, Canada, B3H 4J1. email: jinyu.sheng@dal.ca

(Figure 1). Its existence has been confirmed by geostrophic calculation, direct current measurements, and infrared satellite images of sea surface temperature [e.g., El-Sabh, 1976; Tang, 1980; Benoit et al., 1985; Mertz et al., 1988]. Previous studies suggested [Koutitonsky and El-Sabh, 1985] that freshwater runoff from the St. Lawrence River system drives a buoyant estuarine plume in the St. Lawrence Estuary, with two separate coastal currents flowing eastward along the north and south shores, respectively. Combined with the cyclonic circulation of the northwestern Gulf of St. Lawrence, the north shore current in the estuary veers anticyclonically at the estuary mouth and flows southward. It joins the south shore current at the coast, forming the root of the Gaspé Current. The Gaspé Current reaches its highest intensity of about 1 m s^{-1} around the Gaspé Peninsula with a typical width of about 10-20 km in the top 50 m of the water column [Tang and Bennet, 1981]. It apparently leaves the coast at the eastern tip of the Gaspé Peninsula and carries buoyant estuarine waters onto the Magdalen Shallows.

The strength and position of the Gaspé Current varies significantly with

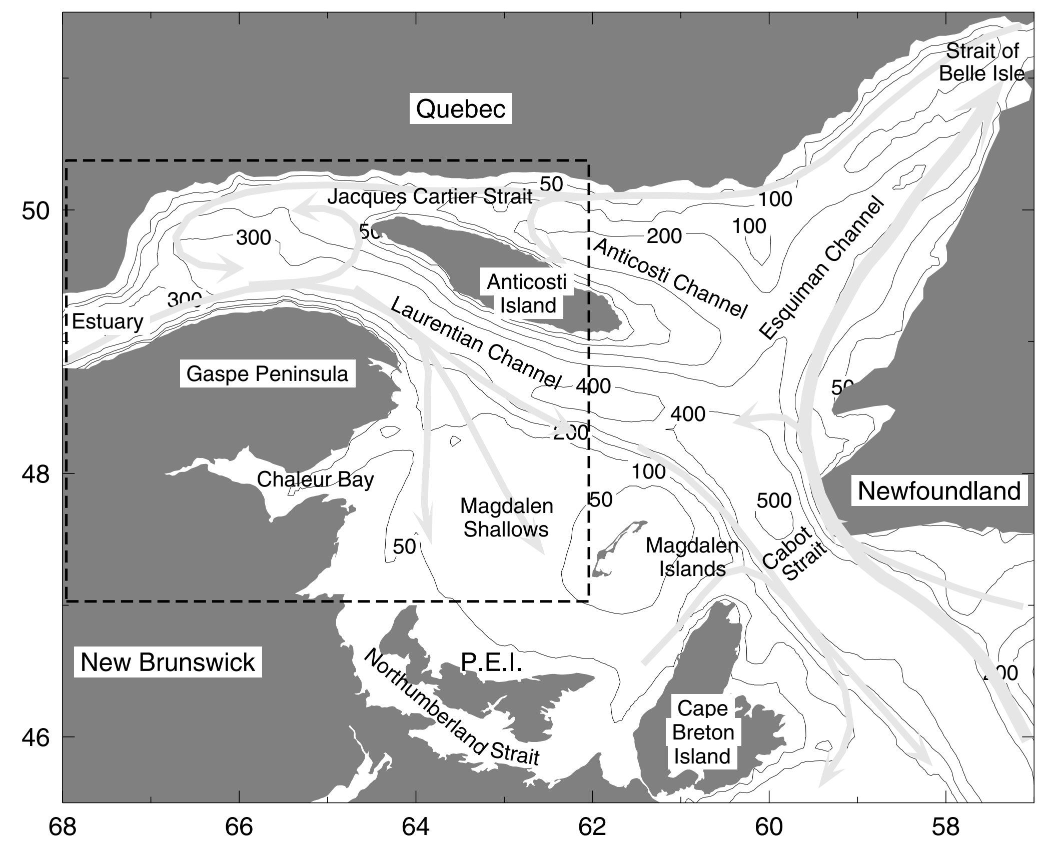

Figure 1. Main bathymetric features of the Gulf of St. Lawrence and a schematic showing the major surface currents. The area marked by the dashed lines is the model domain.

time and space. From satellite infrared images, Tang [1980] was the first to identify the occurrence of instabilities in the Gaspé Current under the summer, high-runoff conditions. The dynamics of the unstable wave development in the Gaspé Current are not yet fully understood. The main objectives of this paper are (1) to study the development of the Gaspé Current and the associated unstable wave features driven by buoyancy forcing associated with the freshwater runoff, and (2) to examine the combined effects of the river discharge and a barotropic westward jet along the Quebec shore on the formation of a large-scale cyclonic motion over the northwest Gulf of St. Lawrence, using a three dimensional eddy-resolving ocean model known as CANDIE [Sheng et al., 1998].

The arrangement of this paper is as follows. The next section summarizes the main features of oceanographic observations over the northwestern Gulf of St. Lawrence in the summer months. This is followed by a description of model configurations used in the numerical experiments. It then presents the model results in an idealized basin that consists of a flat bottom and a piecewise-straight coastline and in a realistic domain of the northwest Gulf of St. Lawrence. The final section is a summary and conclusions.

Review of Oceanographic Observations

Freshwater discharge from the St. Lawrence plays a dominant role in driving circulation over the northwestern Gulf of St. Lawrence (NWGSL). The annual mean discharge of the St. Lawrence is about 0.018 Sv (1 Sv = 10^6 m^3 s^{-1}), with significant seasonal variations. During the period from 1950 to 1984, for example, the monthly mean runoff of the St. Lawrence was about 0.015 Sv from September to March of the next year, but increased to more than 0.03 Sv in May and June [Koutitonsky and Bugden, 1991]. The peak runoff from the St. Lawrence in later spring is most likely to trigger the development of meanders and instabilities in the Gaspé Current during the summer season. Therefore in this paper we only discuss the summer mean climatology of temperature and salinity and use them to initialize the model.

Figure 2 shows the summer surface temperature and salinity over the northwestern Gulf of St. Lawrence (the area marked by the dashed lines in Figure 1). They were gridded using a successive-correction method known as Barnes' Algorithm [Daley, 1991] from the hydrographic observations made at depths of less then 11 m during the summer months (July-September). The results presented in Figure 2 are based on three iterations and an influence radius of about 15 km.

The surface water in summer warms up progressively from the southwestern shallow area to the northern part of the NWGSL, with the coldest water around the estuary mouth and northern part of Jacques Cartier Strait. Along the Gaspé Peninsula, however, the summer surface temperature is relatively uniform. By contrast, the summer surface salinity varies significantly around the estuary mouth and the coastal region of the Gaspé Peninsula, with lower salinity closer to the shore. The combination of strong cross-shore variations in the summer surface salinity and relatively weak variations in the summer surface temperature along the Gaspé Peninsula indicates the predominance of the salinity distribution in driving the buoyancy-driven coastal current, i.e. the Gaspé Current, in the summer season.

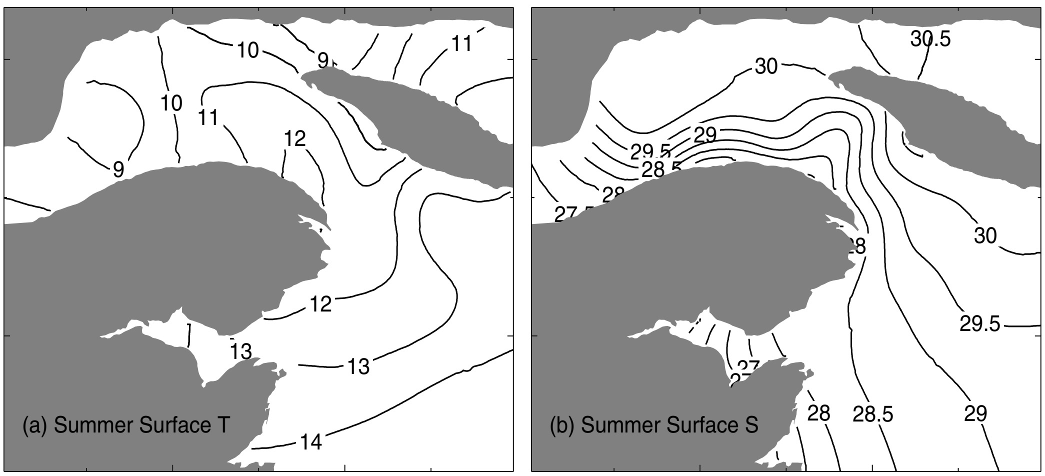

Figure 2. Summer mean surface (0-11m) fields of (a) temperature and (b) salinity gridded from hydrographic data using Barnes' algorithm [Daley, 1991].

Figure 3a presents vertical profiles of summer-mean temperature and salinity. They were obtained by horizontally averaging the three-dimensional gridded summer-mean temperature and salinity over the NWGSL. The water column over this region in summer can be described as a three-layer system: a warm and relatively fresh surface layer, a cold intermediate layer, and a warmer and saltier bottom layer. Figure 3b presents the vertical profile of density calculated from temperature and salinity profiles shown in Figure 3a. The density difference between the surface and at a depth of 250 m is about $5\sigma_t$ (i.e. 5×10^3 kg m^{-3}), which is quite large. By assuming the horizontal scale of motion to be much larger than the vertical scale and ignoring the nonlinear terms, we calculated the baroclinic modes using the method outlined by Kundu [1990]. Figure 3c shows the pressure eigenfunctions of the first three baroclinic modes. The phase speeds c_i of the first three modes are about 0.99, 0.55 and 0.37 m s^{-1}, respectively. The corresponding baroclinic Rossby radii of deformation $r_i = c_i/f$ are about 10, 5.5 and 3.7 km, respectively, where f is the Coriolis parameter.

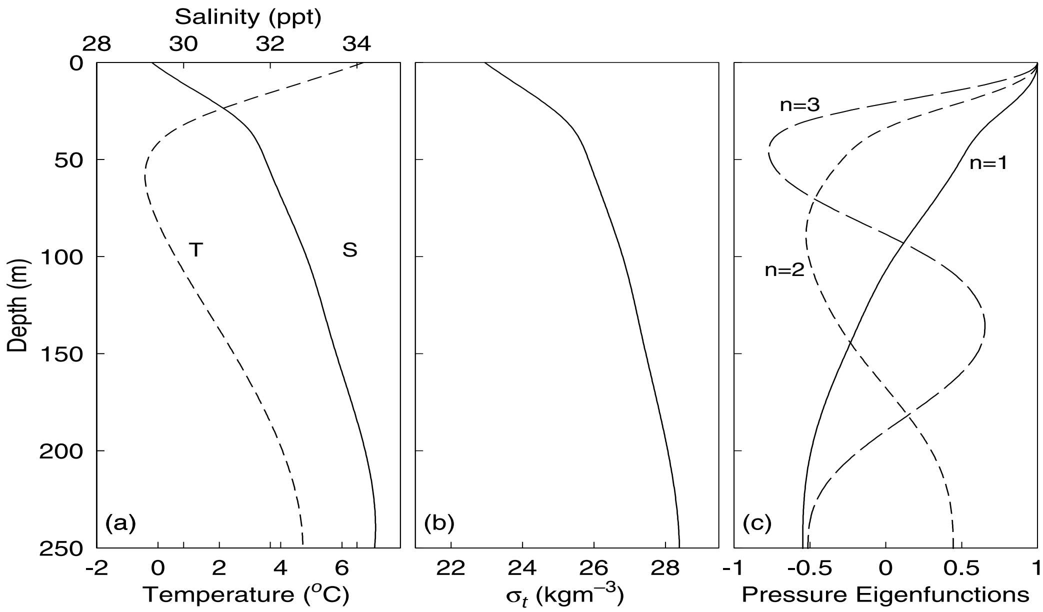

Figure 3. Vertical profiles of (a) temperature and salinity spatially averaged from the gridded hydrographic data over the northwestern Gulf of St. Lawrence, (b) in situ density calculated from the vertical temperature and salinity profiles shown in (a), and (c) pressure eigenfunctions of the first three baroclinic modes calculated based on the vertical density profile shown in (b).

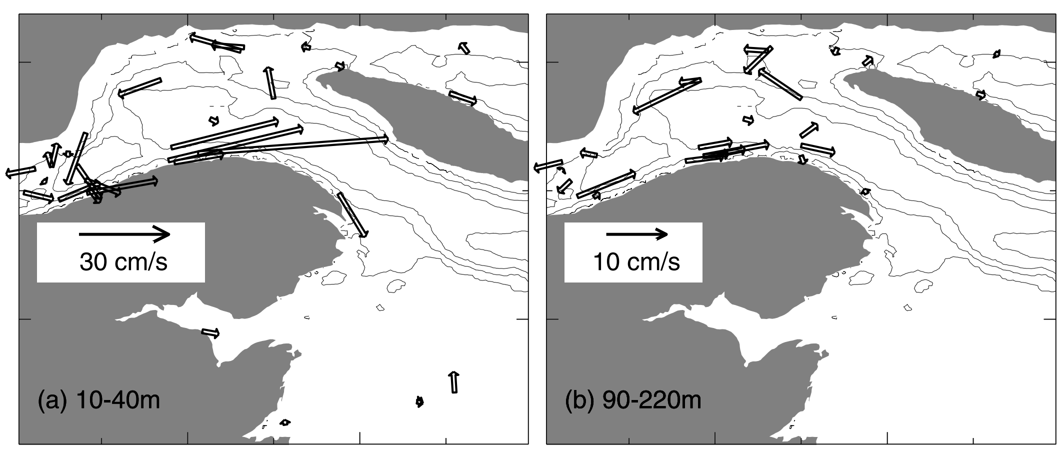

Figure 4. Time mean current-meter observations made during the summer months with record lengths longer than 15 days in the (a) upper-ocean (10-40 m) and (b) lower-ocean (90-220 m) over the northwestern Gulf of St. Lawrence.

Figure 4 shows the time mean current-meter observations made during the summer months with record lengths longer than 15 days in the upper-ocean (10 to 40 m) and in the lower-ocean (90 to 220 m), respectively. The tides were removed before calculating the mean [Gregory et al., 1989]. Horizontal averaging was performed where means were available within 10 km of each other. The summer mean upper-ocean current-meter observations exhibit significant spatial variabilities, particularly near the mouth of the estuary (Figure 4a). Nevertheless, they suggest a transverse flow with typical speed of about 10 cm s^{-1} around the estuary mouth and a strong coastal current (i.e. the Gaspé Current) with the maximum time-mean speed of about 50 cm s^{-1} along the Gaspé Peninsula in the upper-ocean during the summer season. They also suggest a large-scale cyclonic motion in the upper-ocean over the NWGSL region in summer months. The summer mean current-meter observations in the lower-ocean (Figure 4b) are much weaker than those in the upper-ocean, particularly over the estuary mouth and along the Gaspé Peninsula, indicating the surface-intensified characters of the Gaspé Current and the cyclonic NWGSL circulation.

Model Description

The governing equations used in the ocean circulation model are essentially the same as those considered by Sheng et al. [1998], with the exception that Cartesian coordinates are used here.

$$\frac{\partial u}{\partial t} + \mathcal{L}u - fv = -\frac{1}{\rho_o}\frac{\partial p}{\partial x} + \mathcal{D}_m u + \frac{\partial}{\partial z}\left(K_m \frac{\partial u}{\partial z}\right), \tag{1}$$

$$\frac{\partial v}{\partial t} + \mathcal{L}v + fu = -\frac{1}{\rho_o}\frac{\partial p}{\partial y} + \mathcal{D}_m v + \frac{\partial}{\partial z}\left(K_m \frac{\partial v}{\partial z}\right), \tag{2}$$

$$\frac{\partial p}{\partial z} = -\rho g, \tag{3}$$

$$\frac{\partial u}{\partial x} + \frac{\partial v}{\partial y} + \frac{\partial w}{\partial z} = 0, \tag{4}$$

$$\rho = \rho(T, S, p), \tag{5}$$

$$\frac{\partial T}{\partial t} + \mathcal{L}T = \mathcal{D}_h T + \frac{\partial}{\partial z}\left(K_h \frac{\partial T}{\partial z}\right), \tag{6}$$

$$\frac{\partial S}{\partial t} + \mathcal{L}S = \mathcal{D}_h S + \frac{\partial}{\partial z}\left(K_h \frac{\partial S}{\partial z}\right), \tag{7}$$

where u, v, w are east (x), north (y) and vertical (z) components of the velocity, p is pressure, ρ is density, g are the gravitational acceleration, ρ_o is a reference density, and K_m and K_h are the vertical eddy viscosity and diffusivity coefficients. Here $\mathcal{L}$ is an advection operator and $\mathcal{D}_m$ and $\mathcal{D}_h$ are diffusion operators defined as

$$\mathcal{L}q = u\frac{\partial q}{\partial x} + v\frac{\partial q}{\partial y} + w\frac{\partial q}{\partial z}, \qquad \mathcal{D}_{m,h}q = A_{m,h}\left(\frac{\partial^2 q}{\partial x^2} + \frac{\partial^2 q}{\partial y^2}\right) \tag{8}$$

where A_m and A_h are the horizontal eddy viscosity and diffusivity coefficients, respectively. In this paper, surface wind and surface heat/salinity fluxes were set to zero, the vertical mixing coefficients K_m and K_h were set to 1 cm^2 s^{-1}, and horizontal eddy viscosity and diffusivity coefficients $A_{m,h}$ were determined using the Smagorinsky scheme [Smagorinsky, 1963].

Two types of model domains were used in this study. The first is an idealized basin with a flat bottom and a piecewise-straight coastline (Figure 5a). The dimension of the rectangular estuary is about 40 km wide and 70 km long. The water depth of this idealized basin is 200 m. The second model domain type is a realistic basin with a variable bottom and an irregular coastline, representing the model-resolved bathymetry over the NWGSL region. The water depth at the estuary head in both the idealized and realistic basins was set to 30 m for implementing a source of lower-salinity waters in the model.

The model resolution is about 3.0 km in the east-west direction and 2.3 km in the north-south direction with twenty z-levels in the vertical. The vertical grid spacing in the idealized basin is uniformly 10 m. In the realistic basin the vertical grid spacing is uniformly 10 m from surface to 140 m. Below 140 m the vertical cell boundaries are at depths of 152, 168, 189, 218, 257, and 310 m, respectively.

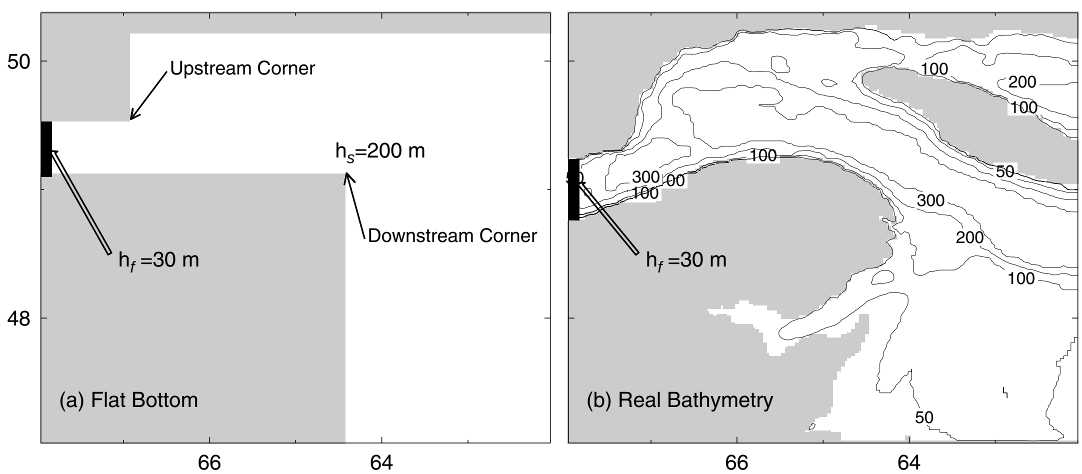

Figure 5. Two types of model domains used in the numerical experiments. (a) The idealized basin of a flat bottom and a piecewise-straight coastline. The water depth of this basin is 200 m except the estuary head region where the water depth is 30 m. (b) The realistic basin with variable bottom and irregular coastline representing the model resolved bathymetry over the area marked by the dashed lines in Figure 1.

At the model lateral closed boundaries, the normal flow, tangential stress of the currents and horizontal fluxes of temperature and salinity were set to zero. The areas with nonzero depths along the eastern and southern boundaries (Figure 5) are the model open boundaries. Along these boundaries the Sommerfeld radiation condition was applied for normal flow, temperature and salinity fields at each model level.

The model was initialized with the summer mean vertical profiles of temperature and salinity shown in Figure 3a with zero initial velocity everywhere except the estuary head. The time step is $\Delta t = 432$ s, or 200 steps per day. To simulate the summer mean St. Lawrence River runoff in the model, we specified the water mass at the estuary head to be 10 ppt fresher than the summer mean salinity at each z-level. We also prescribed a weak barotropic eastward inflow of 2.5 cm s^{-1} at the head to represent the summer mean volume transport of 0.03 Sv from the St. Lawrence River system.

Idealized Basin Experiments

CANDIE was first applied to the idealized basin forced by the St. Lawrence River discharge specified in terms of lower salinity waters and a weak barotropic eastward flow at the estuary head. Shortly after the model initialization, a zonal pressure gradient is created due to the density difference around the estuary head. This zonal pressure gradient drives an eastward surface current that advects the buoyant estuarine water downstream over the whole head region. Due to the Coriolis effect, this surface current veers southward and forms a strong southward jetlike stream along the offshore front of the estuarine plume (Figure 6a). At the north and south shores of the estuary, the Coriolis term in the zonal momentum equation vanishes, leading to a balance between the zonal pressure gradient and the inertial terms in the momentum equation over these two areas (since the dissipative terms are relatively small). Consequently, the buoyant estuarine waters along both shores spread gradually eastward. The southward jetlike stream along the offshore front of the plume turns cyclonically at the south shore, forming a narrow coastal current that flows eastward along the right-bounded coast (Figure 6a). The model-produced onset of the plume-current system in this idealized basin is very similar to that observed in the "dam-break" laboratory experiment [Stern et al., 1982] and produced by numerical models of buoyancy-driven circulation in a channel [Wang, 1985; Chao and Boicourt, 1986].

The coastal current driven by the river discharge is stable initially (Figure 6a). Due to strong horizontal and vertical shears, however, instabilities start to develop around day 10 (Figure 6b). Figure 7 presents the time sequence of surface salinity and flow fields produced by the fully-nonlinear CANDIE model. The plume-current system has become well developed after 20 days of simulation (Figure 7a), with a pool of accumulated estuarine waters and an intense semi-circular anticyclonic eddy at the downstream corner. The surface current inside the anticyclonic eddy abruptly turns cyclonically at the coast to south of the corner, acting as a transition zone connecting the eddy and the coastal current farther south [Chao and Boicourt, 1986].

After 40 days of simulation (Figure 7b), the offshore salinity front of the plume expands further downstream with a small-scale anticyclonic gyre generated inside the plume. The anticyclonic eddy at the downstream corner has grown into a very large size with its center about 50 km northeastward from the corner. The other interesting feature in Figure 7b is the development of several backward-breaking waves along the piecewise-straight coastline, with one well-defined wave about halfway between the estuary mouth and the downstream corner, and two other smaller waves to the south of the corner.

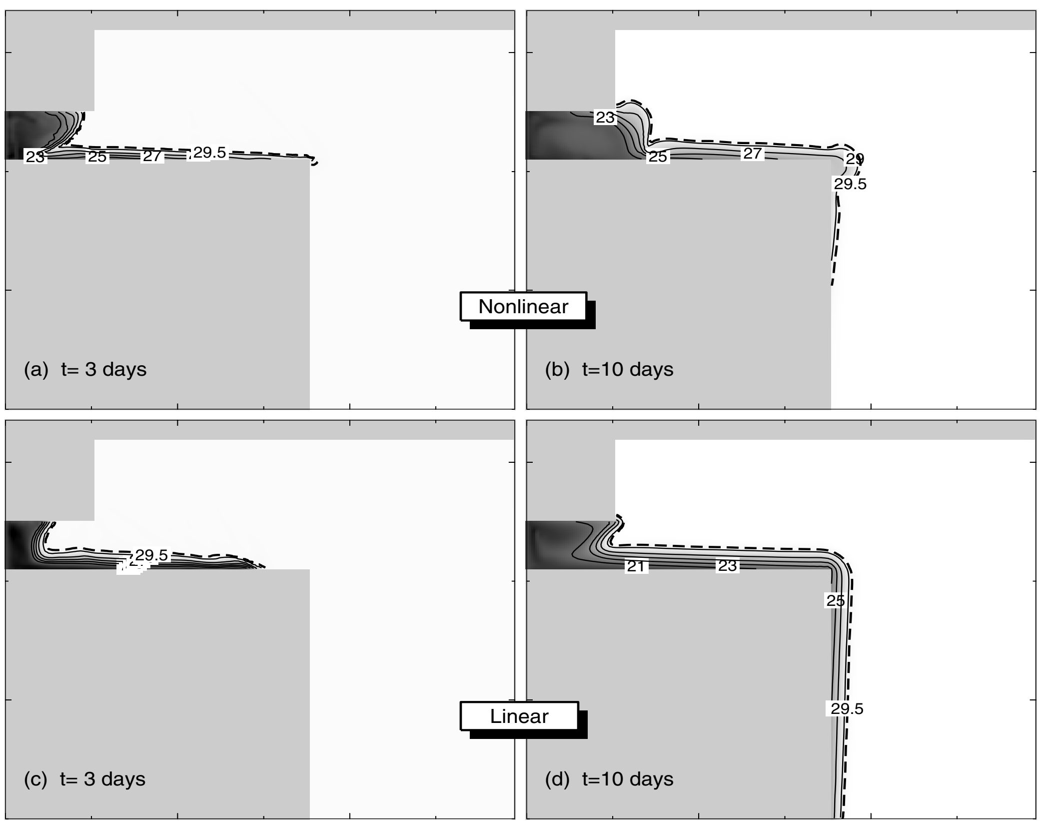

Figure 6. Grayscale images and isopleths of surface salinity fields in the idealized basin produced by the fully-nonlinear model at (a) day 3 and (b) day 10; and those produced by the linearized model (i.e. the momentum advection terms in the model are dropped) at (c) day 3 and (d) day 10. Both numerical experiments were forced by the same river discharge at the estuary head. Darker gray represents lower salinity. The salinity contour interval is 2 ppt. The dashed contour line represents the boundary between the buoyant estuarine and shelf waters.

The well-defined backward-breaking wave has broken upstream and dissipated by day 60, creating a pool of buoyant estuarine waters to the northeast of the upstream corner (Figure 7c). The backward-breaking wave to the south

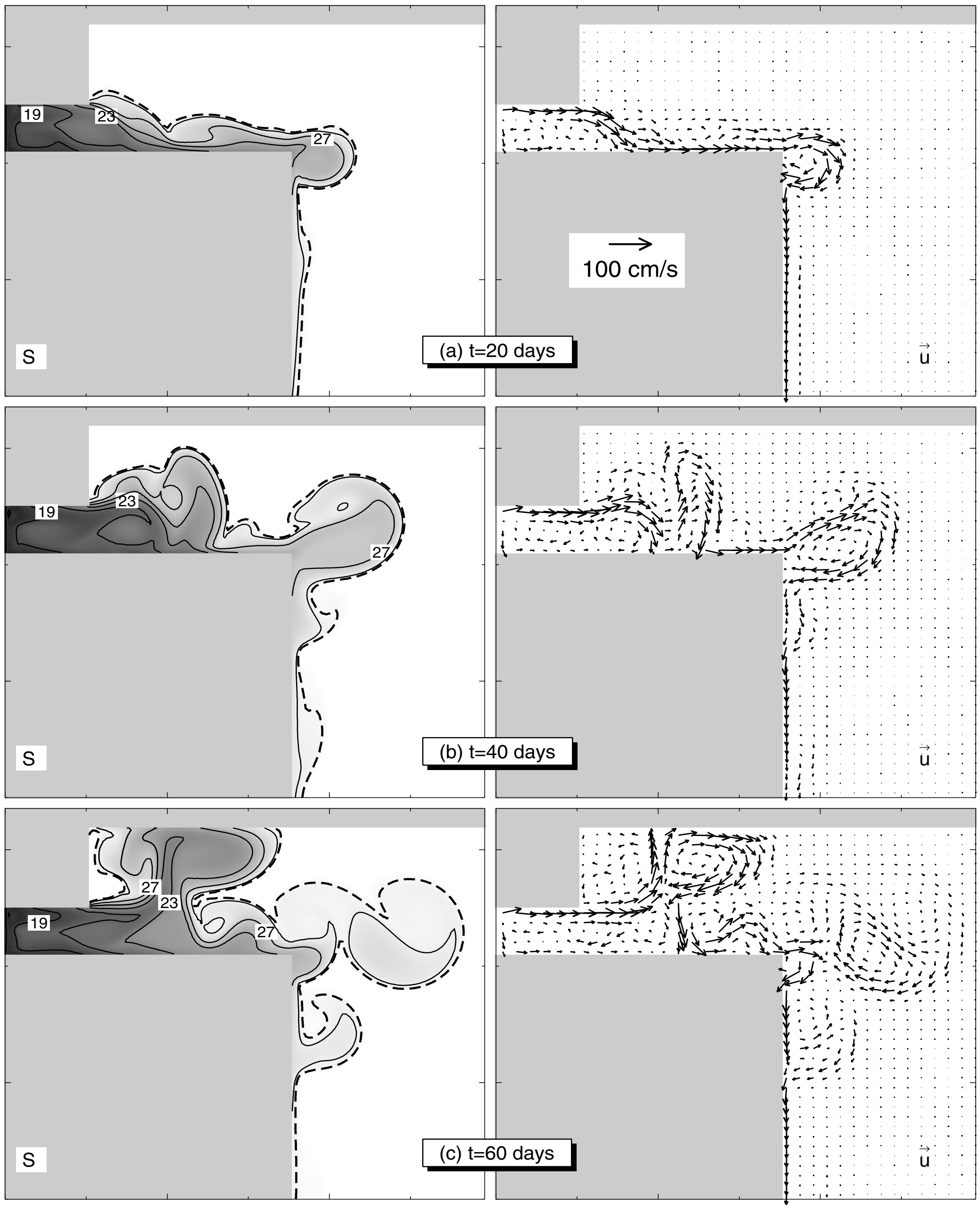

Figure 7. Surface salinity and flow fields in the idealized basin produced by the nonlinear model at (a) day 20, (b) day 40 and (c) day 60. The model was driven by the river discharge at the estuary head. The salinity contour interval is 2 ppt. The dashed salinity contour line represents the boundary between estuarine and shelf waters. Velocity vectors are shown at every fourth grid point.

of the downstream corner enlarges and will break away shortly from the plume-current system (see Figures 7c). Figure 7c also shows that the anticyclonic eddy at the downstream corner has been pinched off from the plume-current system by day 60, with a new anticyclonic eddy created at the downstream corner. This eddy-shedding phenomenon is consistent with the laboratory simulations by Klinger [1994]. He observed that an anticyclonic eddy is always formed when the current, which flows with the coast to its right if one is oriented in the downstream direction on the northern Hemisphere, encounters a sharp convex corner with an angle greater than about 45°. He also found that this eddy grows in size and propagates diagonally away from the corner. As this eddy moves away from the corner, a new anticyclonic eddy is created.

Note that the nonlinear advective terms in the horizontal momentum equations (i.e., $\mathcal{L}u$ and $\mathcal{L}v$ terms) play a predominant role in the development of meanders and instabilities in the plume-current system. Figures 6c and 6d present the surface salinity fields at days 3 and 10 produced by the CANDIE model with the momentum advection terms eliminated. We refer to this type of experiment as the linear case. The overall features of surface salinity and flow in the linear case are similar to those in the nonlinear case (i.e. the results produced by the fully-nonlinear CANDIE model), however, the coastal current in the linear case flows smoothly along the coast without meanders or backward-breaking waves.

Realistic Basin Experiments

The fully nonlinear CANDIE model was applied to the realistic basin forced by the same river discharge as in the idealized basin. All other model parameters are the same as before. Figure 8 shows surface salinity fields at days 3 and 10 in the realistic basin. After 3 days, the buoyant estuarine plume is confined inside the St. Lawrence Estuary with a semicircular salinity front near the mouth. A weak coastal current has just been created over the south shore of the Estuary, advecting the buoyant estuarine waters eastward along the Gaspé Peninsula. A westward intrusion occurs between the salinity front and the south shore near the mouth, very similar to that in the idealized basin.

A comparison of Figure 8a with Figure 6a indicates that the surface salinity and current fields in both idealized and realistic basins have qualitatively similar spatial structures at day 3: a buoyant plume inside the estuary, a semi-cyclonic front around the estuary mouth and a surface-intensified coastal current along the right-bounded coast. Note, however, that the intrusion speed during the first three days of simulation is much slower in the realistic basin (about 0.58 m s^{-1}) than that in the idealized basin (about 1.0 m s^{-1}). The coastal current in the realistic basin is also relatively weaker during this period.

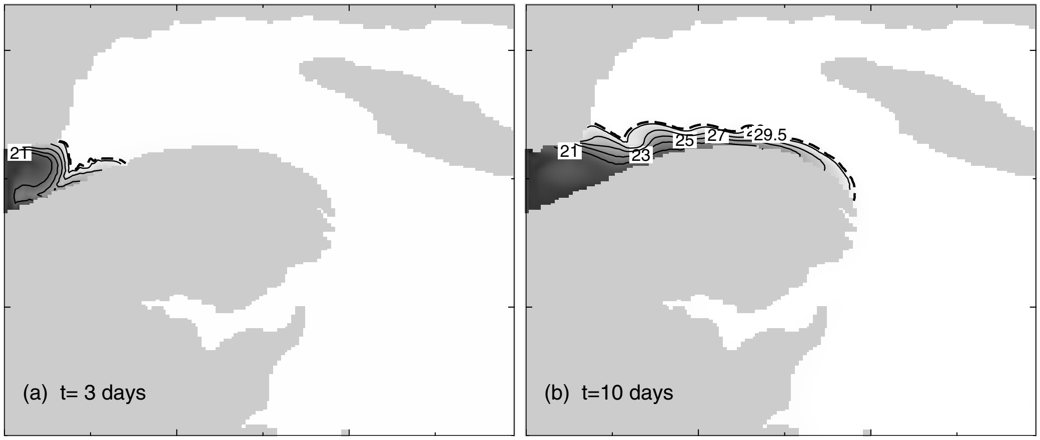

Figure 8. Grayscale images and isopleths of the surface salinity fields in the realistic basin produced by the fully-nonlinear CANDIE model at (a) day 3 and (b) day 10. Otherwise, same as Figure 6.

After 10 days the coastal current in the idealized basin is relatively stable with a small-scale anticyclonic eddy just created at the downstream corner (Figure 6b). By contrast, the coastal current in the realistic basin flows along the irregular coastline without any recognizable separation (Figure 8b). Note that large-scale meanders appear along the outer edge of the coastal current in the realistic basin, indicating that the plume-current system is more unstable in the realistic basin than in the idealistic basin.

Figure 9 shows the evolution of surface salinity and currents in the realistic basin. After 20 days, the meanders along the outer edge of the coastal current grow in size and form several large backward-breaking waves with a typical wavelength of about 50 km. By comparison, the coastal current in the idealized basin is relatively stable at this time with two small-scale backward-breaking waves created along the outer edge of the current (Figures 7a and 9a). The intense anticyclonic eddy appearing at the downstream corner of the idealized basin is not present in the realistic basin. Instead, the coastal current in the realistic basin tends to generate several smaller-scale anticyclonic eddies along the irregular coastline.

The buoyant plume in the realistic basin expands northeastward significantly after 40 days of simulation, with a cyclonic-anticyclonic dipole created to the northeast of the estuary mouth (Figure 9b). The coastal current separates from and reattaches to the irregular coastline sporadically as it propagates downstream. After passing the eastern tip of the Gaspé Peninsula, the current leaves the coast permanently and flows southward onto the Magdalen Shallows. By comparison, the buoyant plume in the idealized basin also expands further eastward but with a small-scale anticyclonic eddy inside the plume and a large-scale backward-breaking wave outside the plume.

At day 60, the buoyant estuarine water in the realistic basin spreads over most of the NWGSL region with an intense anticyclonic eddy to the northeast of the estuary mouth (Figure 9c). A small-scale but well-developed anticyclonic eddy is created over the area between the eastern tip of the Gaspé

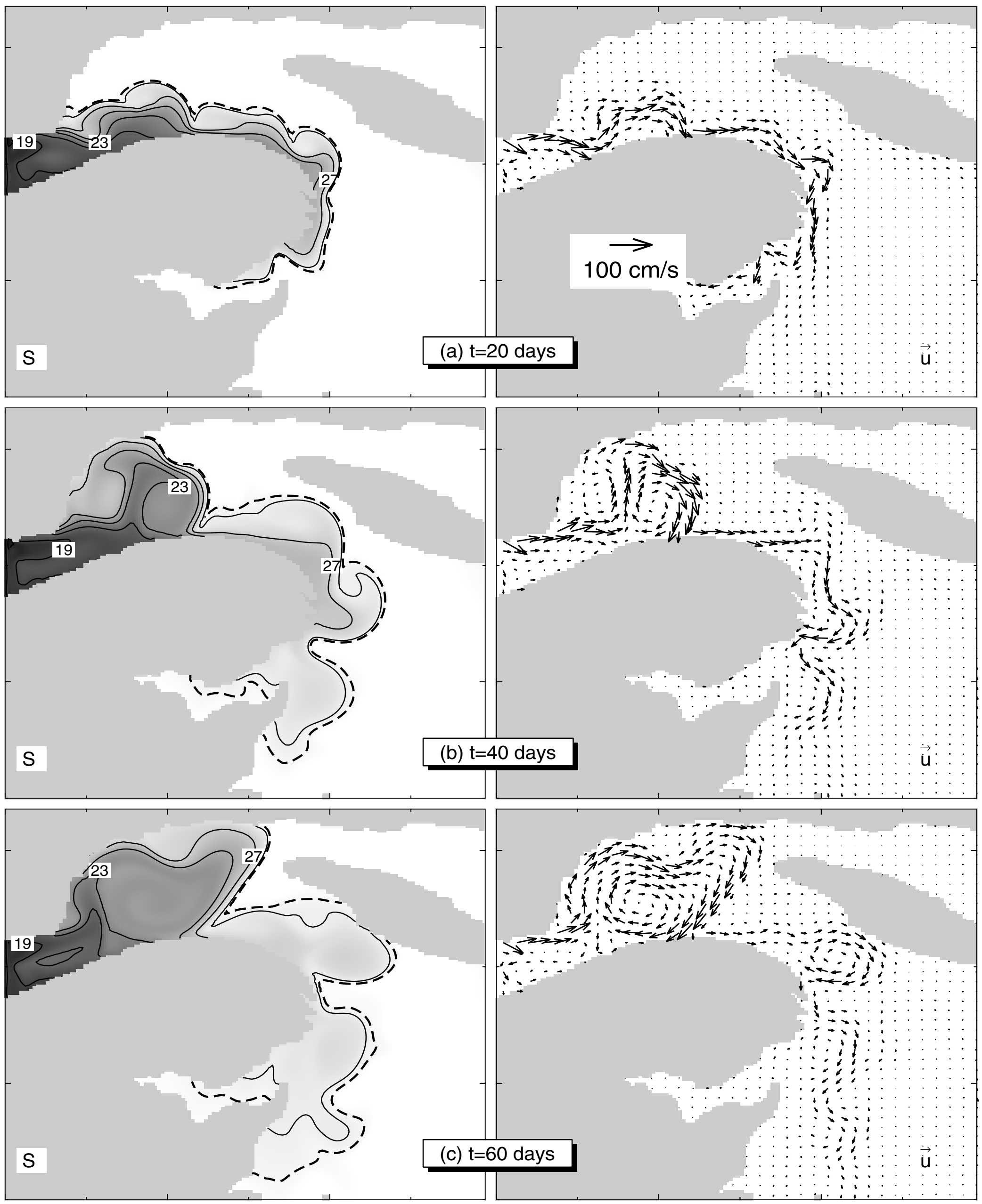

Figure 9. Surface salinity and flow fields in the realistic basin driven by the river discharge at the estuary head at (a) day 20, (b) day 40, and (c) day 60. Otherwise, same as Figure 8.

Peninsula and Anticosti Island. To the south of this eddy several less well developed eddies have been created with a southward drift onto the Magdalen Shallow. By contrast, in the idealized basin a pool of buoyant water tends to separate from the plume-current system.

The model results shown in Figure 9 reproduce many observed features of the Gaspé Current, including the development of backward breaking waves frequently observed in the satellite infrared images [Tang, 1980; Mertz et al., 1988]. As discussed above, however, the buoyant estuarine plume driven by the river discharge expands progressively eastward with time. As a result, a large-scale anticyclonic motion is eventually created over the NWGSL region. This anticyclonic motion produced by the model is, however, contrary to common knowledge of general circulation over this region. Previous hydrographic studies have consistently revealed the presence of a quasi-permanent geostrophic cyclonic motion in this region [Trites, 1972; El-Sabh, 1976; Tang, 1983]. The summer mean current meter observations in the upper ocean (Figure 4) also suggest the existence of this circulation feature. Clearly, other dynamic processes in addition to the St. Lawrence River discharge are involved in the formation of the cyclonic circulation over the NWGSL region. In this section, we consider the role of a barotropic westward jet along the Quebec shore in the formation of the cyclonic NWGSL motion. This is motivated by the findings of Petrie et al. [1988], showing that the Labrador Current enters the Gulf of St. Lawrence through the Strait of Belle Isle with volume transport up to 0.3 Sv. These Labrador Current waters are thought to flow westward along the Quebec shore and are entrained into the cyclonic circulation in the northwest Gulf region.

The fully-nonlinear CANDIE model was then applied to the realistic basin forced by both the river discharge at the estuary head and a barotropic westward jet at the northeast corner of the eastern open boundary. The speed and width of the boundary inflow are about 8 cm s^{-1} and 40 km respectively, corresponding to the volume transport of about 0.3 Sv. The salinity and temperature of this jet are the same as the initial fields. Other model parameters are the same as before. Figure 10 shows the surface salinity and current fields at days 20, 40 and 60.

The addition of the boundary inflow introduces significant variations in the plume-current system and the associated eddy and meander development. Figure 10a shows a weak westward coastal current along the Quebec shore as a direct result of this boundary inflow. The current becomes relatively stronger as it flows through the Jacques Cartier Strait and joins the estuarine outflow at the estuary mouth, forming the root of the surface-intensified Gaspé Current (Figure 10a).

A comparison of the model results in Figures 9b and 10b clearly shows that the westward coastal current along the Quebec shore effectively constrains the eastward expansion of the buoyant estuarine plume, resulting in more estuarine waters advected seaward, and strengthens the Gaspé Current along the Gaspé

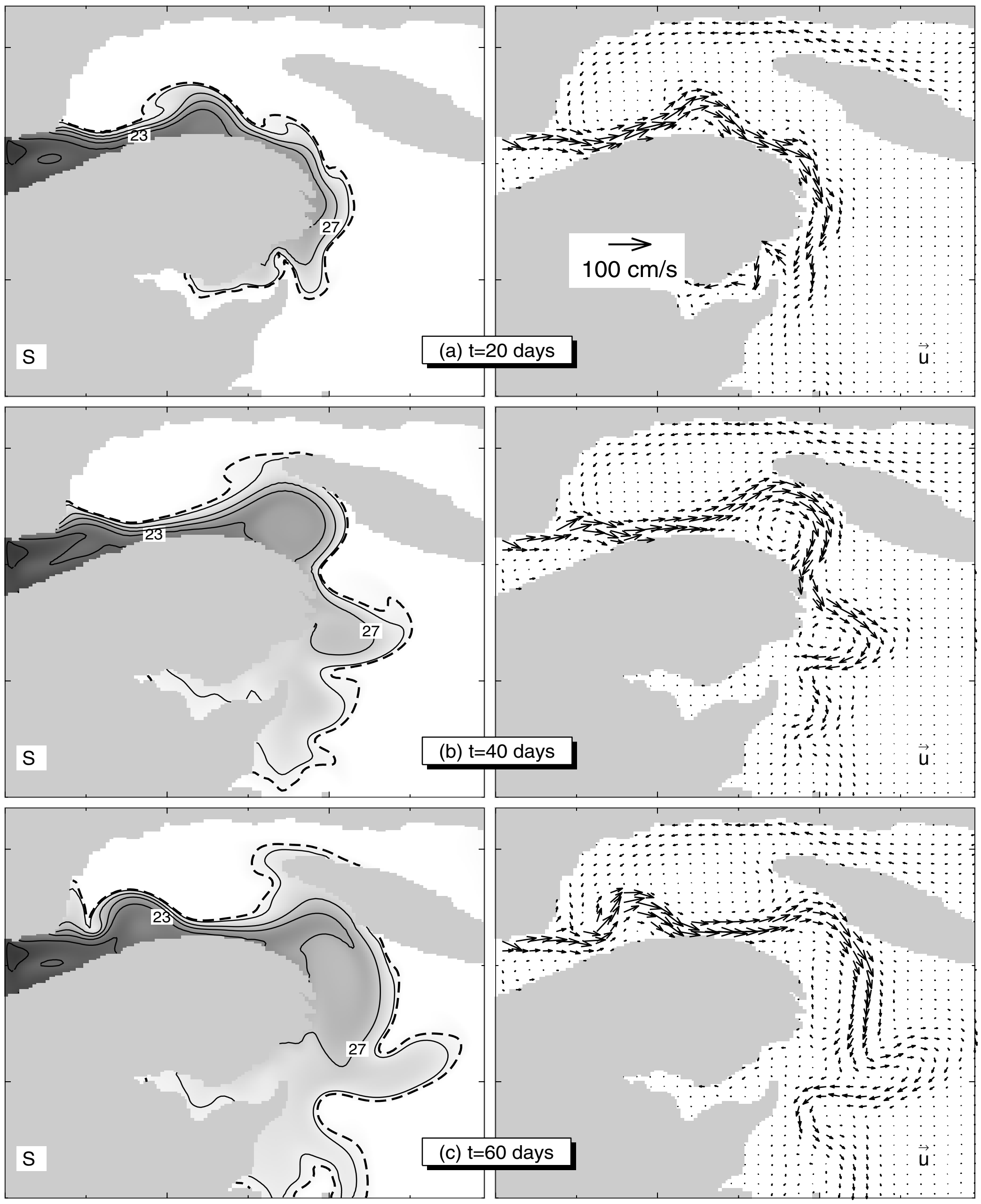

Figure 10. Near surface salinity and flow fields in the realistic basin forced by the river discharge at the estuary head and a barotropic westward inflow at the northeast corner of the eastern open boundary at (a) day 20, (b) day 40 and (c) day 60. Otherwise, same as Figure 9.

Peninsula. Furthermore, the combination of the westward coastal current along the Quebec shore and the eastward Gaspé Current along the Gaspé Peninsula forms a large-scale cyclonic circulation over the NWGSL, agrees qualitatively with the time-mean current observations presented in Figure 4.

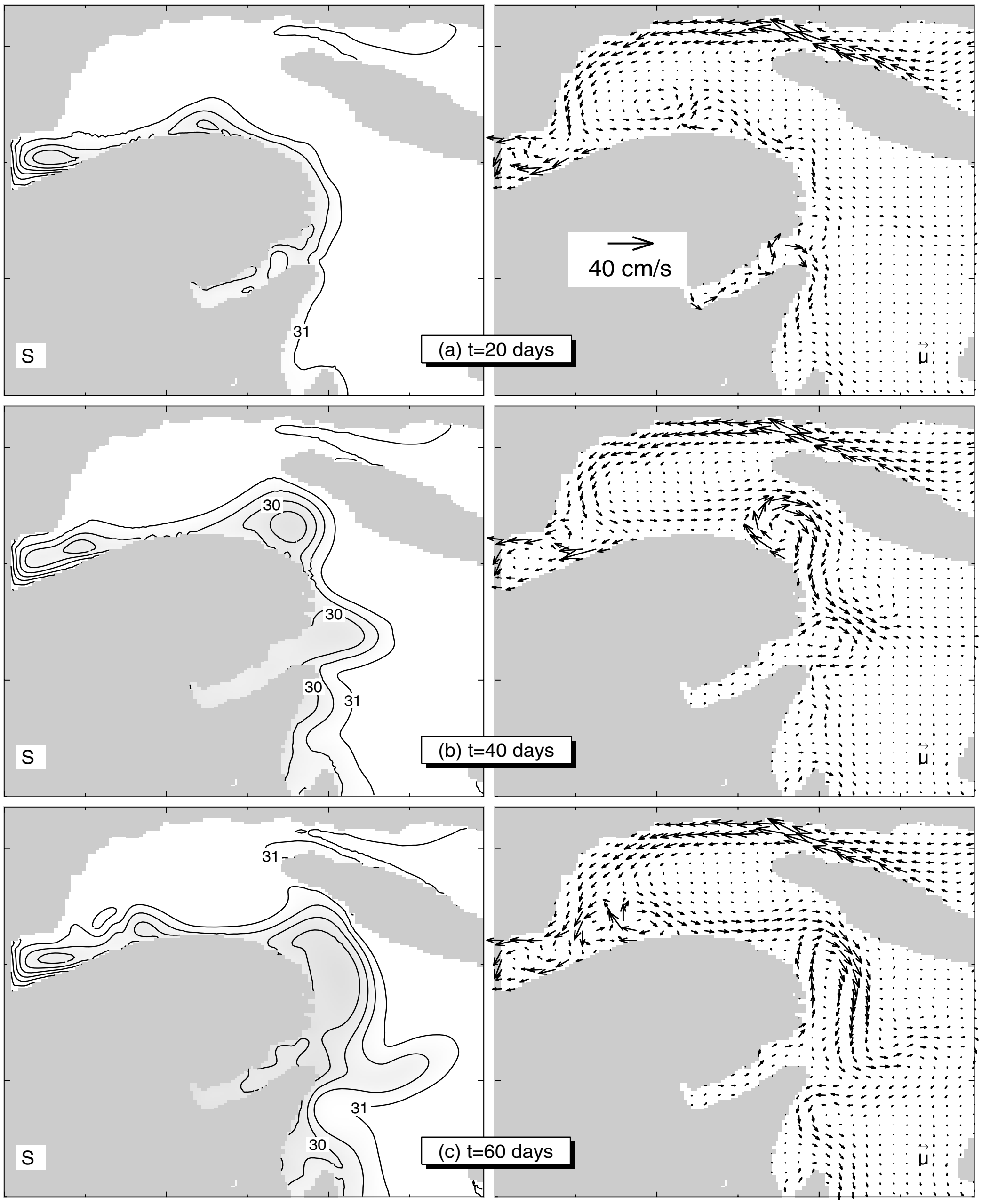

Figure 11. Sub surface salinity and flow fields on the fourth model level centered at 35 m in depth in the realistic basin at (a) day 20, (b) day 40 and (c) day 60. The salinity interval is 0.5 ppt. Otherwise, same as Figure 10.

Figure 10 shows that, initially, the Gaspé Current also flows closely along the irregular coastline. Due to the combining effects of the momentum advection, boundary inflow, and curvature of the coastline, however, a small amount of buoyant estuarine waters are accumulated around the northernmost tip of the Gaspé Peninsula at day 20, with a wavelike feature appearing along the outer edge of the Gaspé Current (Figure 10b). At day 40, a significant amount of estuarine waters are accumulated over the area between the Gaspé Peninsula and Anticosti Island, resulting in an intense anticyclonic eddy over this area (Figure 18b). To the south of this eddy, the Gaspé Current separates from and reattaches to the coast sporadically as it propagates southward. After 60 days, the Gaspé Current separates completely from the coast after passing the northernmost tip of the Gaspé Peninsula, creating an offshore jet that flows onto the Magdalen Shallows with large-scale meanders.

Figure 11 shows the time sequence of salinity and flow fields on the fourth model level centered at 35 m. The sub-surface salinity variations occur mainly along the Gaspé Peninsula and the adjacent coastal and estuary areas with several recognizable pools of lower-salinity waters. These pools of lower salinity waters are highly coherent with the anticyclonic motions. The coastal current along the Quebec shore at this depth is relatively comparable with surface flow. The sub-surface flow along the Gaspé Peninsula, however, is much weaker than at the surface.

Summary and Discussions

This is the first time that a primitive equation model has been used to study the development of the coastal current and the associated eddy and instability generation over the NWGSL region. Two model domains are used in this study. The first is an idealized basin that consists of a flat bottom and piece-wise straight coastlines. The other is the realistic basin of the model-resolved bathymetry over the northwestern Gulf of St. Lawrence. The model results demonstrate that the early development of the plume-current system is qualitatively similar in both the idealized and realistic basins: a buoyant plume is created inside the estuary with a strong eastward surface outflow along the north shore of the estuary. Due to the Coriolis effect, this outflow turns anticyclonically and flows southward along the salinity front of the plume near the estuary mouth. It abruptly turns cyclonically at the south shore to form a surface intensified coastal current that advects the buoyant estuarine water downstream. Due to the combined effects of irregular bathymetry and nonlinear momentum advection, however, the coastal current is relatively weaker and the propagation speed of the intrusion nose is much slower in the realistic basin than those in the idealistic basin. Furthermore, an intense anticyclonic eddy is created at the downstream corner in the idealized basin, that grows in size and finally pinches off from the coast with a new eddy generated at the corner. In the realistic basin, however, the coastal current is more unstable with meanders and backward-breaking waves developing along the outer edge of the current.

With the river discharge as the only driving force, however, the buoyant estuarine plume expands successively with time, leading to a large-size anticyclonic circulation over the NWGSL region. This is opposite to the quasi-permanent cyclonic gyre observed over this area. The addition of a barotropic westward jet specified at the northeast corner of the east open boundary is efficient to constrain the seaward expansion of the estuarine plume and strengthens the Gaspé Current. The combined effect of the river discharge at the estuary head and the westward coastal current along the Quebec shore results in the formation of a statistically-stable cyclonic circulation over the NWGSL region.

Acknowledgments

The author wishes to thank Michael Dowd, Fraser Davidson, Yuyou Lu, Josko Bobanovic, Richard Greatbatch, Keith Thompson, Dan Wright, and Brad DeYoung for their useful suggestions and comments. I am grateful to Brian Petrie, Ken Drinkwater, and Doug Gregory for making hydrographic data and monthly mean current meter data available to me. Thanks also go to Dan Kelley and Allan Goulding for making the Gri-plotting package work on a DEC Alpha machine. This study was supported by the Natural Sciences and Engineering Research Council of Canada and the start-up funding from Dalhousie University.

References

Benoit, J., M. I. El-Sabh, and C. L. Tang, Structure and seasonal characteristics of the Gaspé Current, *J. Geophys. Res.*, 90, 3225-3236, 1985.

Chao, S. Y., and W. C. Boicourt, Onset of estuarine plumes, *J. Phys. Oceanogr.*, 16, 2137-2149, 1986.

Daley, R., *Atmospheric Data Analysis*, Cambridge University Press, 457 pp., 1991.

El-Sabh, M. I., Surface circulation pattern in the Gulf of St. Lawrence, *J. Fish. Res. Board of Can.*, 33, 124-138, 1976.

Gregory, D. N, O. C., Nadeau, and D. Lefaivre, Current Statistics of the Gulf of St. Lawrence and Estuary, *Can. Tech. Rep. Hydrogr. Ocean Sci.*, 120, 178 pp., 1989.

Klinger, B. A., Baroclinic eddy generation at a sharp corner in a rotating system, *J. Geophys. Res.*, 99, 12515-12531, 1994.

Koutitonsky, V. G., and M. I. El-Sabh, Estuarine mean flow estimation revisited: Application to the St. Lawrence Estuary, *J. Mar. Res.*, 43, 1-12, 1985.

Koutitonsky, V. G., and G. L. Bugden, The physical oceanography of the Gulf of St. Lawrence: A review with emphasis on the synoptic variability of the motion, in *The Gulf of St. Lawrence: Small Ocean or Big Estuary?* J.-C. Therriault, ed., *Can. Spec. Publ. Fish, Aquat. Sci., 113*, 57-90, 1991.

Kundu, P. K., *Fluid Mechanics*, Academic Press, San Diego, 638 pp., 1990.

Mertz, G., M. I. El-Sabh, and D. Proulx, Instability of a buoyancy-driven coastal jet: the Gaspé Current and its St. Lawrence Precursor, *J. Geophys. Res.*, 93, 6885-6893, 1988.

Petrie, B., B. Toulany, and C. Garrett, The transport of water, heat and salt through the Strait of Belle Isle, *Atmosphere-Ocean*, 26, 234-251, 1988.

Sheng, J., D. G. Wright, R. J. Greatbatch, and D. E. Dietrich, CANDIE: A new version of the DieCAST ocean circulation model, *J. Atm. and Oceanic. Tech.*, 15, 1414-1432, 1998.

Smagorinsky, J., General circulation experiments with the primitive equation. I. The basic experiment, *Mon. Wea. Rev., 21*, 99-165, 1963.

Stern, M. E., J. A. Whitehead, and B. L. Hua, The intrusion of a density current along the coast of a rotating fluid, blocking waves, *J. Fluid Mech.*, 123, 237-265, 1982.

Tang, C. L., Observation of wavelike motion of the Gaspé Current, *J. Physical Oceanogr.*, 10, 853-860, 1980.

Tang, C. L., and A.S. Bennett, Physical oceanographic observations in the northwestern Gulf of St. Lawrence. Data series BI-D-810–6, Bedford Inst. Oceanogr., Dartmouth, Canada, 127 p., 1981.

Tang, C. L., Cross-front mixing and frontal upwelling in a controlled quasi-permanent density front in the Gulf of St. Lawrence, *J. Physical Oceanogr.*, 13, 1468-1481, 1983.

Trites, R. W., The Gulf of St. Lawrence from a pollution point of view, in *Marine Pollution and Sea Life*, M. Ruivo, ed., FAO, Fishing News Books, London, 59-62, 1972.

Wang, D. P., Numerical study of gravity currents in a channel, *J. Phys. Oceanogr.*, 15, 299-305, 1985.

The Gaspé Current and Cyclonic Motion Over the Northwestern Gulf of St. Lawrence

Jinyu Sheng
Department of Oceanography
Dalhousie University
Halifax, Nova Scotia, Canada, B3H 4J1
email: jinyu.sheng@dal.ca

Key Words:

backward-breaking waves, bouyancy forcing, coastal jet, eddy, Gaspé Current, Gulf of St. Lawrence, instability, momentum advection, plume-current system, river runoff